Available online at www.sciencedirect.com
SCIENCE DIRECT®
Journal of Catalysis 225 (2004) 489–497
JOURNAL OF CATALYSIS
www.elsevier.com/locate/jcat

# Selective CO oxidation in the presence of hydrogen: fast parallel screening and mechanistic studies on ceria-based catalysts

Daniele Tibiletti [a], E.A. Bart de Graaf [b], Siew Pheng Teh [a], Gadi Rothenberg [b], David Farrusseng [a], and Claude Mirodatos [a,*]

[a] *Institut de Recherches sur la Catalyse, CNRS, 2, avenue Albert Einstein, F-69626, Villeurbanne cedex, France*
[b] *Chemical Engineering Department, University of Amsterdam, Nieuwe Achtergracht 166, 1018 WV Amsterdam, The Netherlands*

Received 17 December 2003; revised 24 April 2004; accepted 26 April 2004
Available online 4 June 2004

**Abstract**

An accelerated investigation of various ceria-supported platinum catalysts by means of parallel synthesis and testing reactors is reported. The aim is to discover new catalysts for purifying hydrogen for fuel cells and other applications by studying three reactions: selective CO oxidation in the absence and in the presence of hydrogen (SelO*x*), water–gas shift (WGS), and reverse water–gas shift (RWGS). A set of catalysts is prepared by impregnating platinum on various doped ceria supports. These catalysts display, despite their nearly identical X-ray crystal structures, diverse redox/acidic/basic properties and different selectivities in the three test reactions. The best SelO*x* catalysts are also the most active for WGS/RWGS equilibration. In contrast to the conventional two-stage approach of discovery screening followed by lead optimization, we demonstrate that it is possible to extract valuable mechanistic information directly from the discovery stage. Specifically, we elucidate the elementary steps coupling the SelO*x* and WGS processes and gain insight as to the combined effects of hydrogen presence and cation doping on the CO oxidation reaction.


*Keywords:* Combinatorial catalysis; Doped ceria; Fuel cells; Water–gas shift; CO selective oxidation; Platinum

## 1. Introduction

Fuel cell technology plays a major part in future scenarios of sustainable energy management [1,2]. Proton-exchange membrane (PEM) cells are particularly attractive for small-scale and automotive applications, but they suffer from one major disadvantage: CO contamination in the hydrogen feed poisons the metal electrodes, and concentrations below 10 ppm are required for steady-state operation [3,4]. To fulfill that requirement, the final stage of hydrogen purification generally consists of oxidizing selectively the remaining CO to ppm levels. Selective oxidation of CO at high concentration in the presence of hydrogen is preferred only if these low CO quantities can be achieved.

Metal-catalyzed CO oxidation has been studied in depth during the last century. The classical catalyst is supported Pt, but Pd, Rh, and even Au (as gold clusters [5,6]) can be used [7]. As early as 1922, Langmuir [8] laid the basis for two possible reaction pathways. In the first one, only the metallic surface is involved: both CO and $O_2$ molecules adsorb on the platinum crystallite and react together. In the second one, a CO molecule absorbed on the platinum surface reacts with an oxygen atom adsorbed on the support after spillover steps between the two phases. More recent versions of these mechanisms are more complex [9,10], but the second pathway is a good starting point to understand the following investigation of catalysts containing supports that can activate oxygen, maximizing the catalytic benefits from the support–oxygen interactions.

Ceria-based mixed oxides ($Ce_xM_{1-x}O_y$) are versatile solid oxygen exchangers. At high temperatures (400–800 °C) the redox cycle $Ce^{3+} \Leftrightarrow Ce^{4+} + e^-$ facilitates oxygen storage and release from the bulk fluorite lattice. This makes them ideal candidates for catalytic and/or electrocatalytic

* Corresponding author.
*E-mail addresses:* gadi@science.uva.nl (G. Rothenberg), farrusseng@catalyse.cnrs.fr (D. Farrusseng), mirodatos@catalyse.cnrs.fr (C. Mirodatos).

0021-9517/$ – see front matter 
doi:10.1016/j.jcat.2004.04.031

oxidation applications such as solid–oxide fuel cells [11]. However, the *surface* redox chemistry of ceria is sensitive even at low temperatures to crystal structure defects [12], which can be tuned by substituting some of the Ce cations with ions of different size and/or charge [13,14].

In this paper, we study the effects of doping the ceria support of platinum catalysts for three close reactions: selective CO oxidation in the presence of hydrogen (SelO$x$), water–gas shift (WGS), and reverse water–gas shift (RWGS) using a high-throughput methodology. All of the catalysts are screened for all three reactions. Subsequently, we discuss the possible application of these catalysts under hydrogen-free and hydrogen-rich conditions, as well as the elementary catalytic steps in these systems and the advantages of using high-throughput methods to extract mechanistic information directly from the primary screening stage.

## 2. Experimental

### 2.1. Catalysts

A set of 12 catalysts containing 2 wt% Pt on $Ce_{0.9}M_{0.1}O_x$ was prepared and characterized (where M = Pb, Bi, Zr, V, W, Mo, Y, La, In, Sn, and two combinations of Zr/Bi, respectively).

The supports for catalysts containing only one dopant were prepared using a modified version of the method reported by Inomata and co-workers [15]. The mixed oxides were synthesized directly by boiling ground mixtures of their nitrate precursors under vacuum, followed by calcination, as reported previously [13]. The corresponding metal nitrate hydrate precursors were used, except for $Ce_{0.9}V_{0.1}O_y$, $Ce_{0.9}W_{0.1}O_y$, and $Ce_{0.9}Mo_{0.1}O_y$, where the ammonium vanadate, tungstanate, and molybdate were used and $Ce_{0.9}Y_{0.1}O_y$ and $Ce_{0.9}Sn_{0.1}O_y$, where $YCl_3$ and $SnCl_2$ were used. Supports with the two combinations of Zr/Bi were prepared by impregnation of ceria/zirconia with Bi (referred to as MS) and by homogeneous deposition precipitation of Bi on ceria/zirconia (referred to as HDP).

A 2 wt% Pt (as chloroplatinic acid) was loaded on each support by impregnation, using a Sophas robotic system (Zinsser Analytic). Two milliliters of water was dropped on the support, after which the calculated amount $H_2PtCl_6 \cdot 6H_2O$ soln (0.01 M) was added. The suspensions were stirred for 3 h, dried at 80 °C for 4 h, and then calcined for 3 h at 500 °C (ramp rate 300 °C/h). The catalysts were then pelletized and crushed to get a uniform powder with a grain size range of 400–600 μm.

A dopant-free $Pt/CeO_2$ catalyst containing 2 wt% Pt was prepared as reference system and referred to as Pt/Ce. In order to check the effect of Pt loading, an additional dopant-free system containing 4.75% wt% Pt was prepared using a high surface area ceria powder (180 $m^2/g$) and referred to as 4.75% Pt/Ce.

### 2.2. Fast parallel catalyst testing

All the reactions were performed in a 16-channel parallel plug flow reactor, constructed in house [16], and now commercialized as SWITCH 16 reactor by AMTEC GmbH. Reaction products were monitored by fast-gas chromatography and on-line mass spectrometry. GC analysis was performed on a two-channel Variant microGC CP 2003 instrument equipped with two thermal conductivity detectors. Channel A was used for $H_2$, $O_2$, $N_2$, $CH_4$, and CO separation (MolSieve 5A Plot, with Ar as carrier gas at 80 °C), and channel B for $CO_2$ and $H_2O$ separation (PoraPlot Q, with He as carrier gas at 80 °C). MS analysis was performed using an Inficom CPM instrument. Unless noted otherwise, chemicals were purchased from commercial sources (> 99% pure) and used as received. In each run, one reactor channel was loaded with graphite and was used as a reference, and a channel was loaded with a dopant-free $Pt/CeO_2$ catalyst for comparison. The temperature was varied from 100 to 200 °C, with a 5-min isotherm every 20 °C. The carbon mass balance was calculated by monitoring the effluents from the bypass reactor and was between 98 and 102%. Each catalyst's oxygen-storage capacity (OSC) was quantified by measuring the $H_2$ consumption in transient mode using the parallel reactor under isothermal conditions at various temperatures: the catalyst sample was oxidized in air for 15 min, flushed with $N_2$ and then reacted with a reducing mixture of 10% $H_2$ in He, monitoring continuously the hydrogen consumption by MS for 3 min (all the other catalysts were kept meanwhile under $N_2$ flow). After a cycle was completed the temperature was increased by 20 °C and a new cycle started following the previous experimental sequence. The OSC for a given temperature is given in micromoles $H_2$ consumed per gram catalyst. Additional OSC measurements were carried out by using CO instead of $H_2$, keeping the above procedure unchanged.

### 2.3. Procedure for CO oxidation

The catalysts were tested for the CO oxidation reaction both in the absence and in the presence of $H_2$ (SelO$x$), using the following feed mixtures: 1% CO, 2% $O_2$, and balance $N_2$ and 1% CO, 2% $O_2$, 20% $H_2$, and balance $N_2$, respectively. In both cases the total flow rate was 25.75 mL/min and the gas space velocity (GSV) was 22 $L\,h^{-1}\,g_{cat}^{-1}$). The effect of water was studied using a feed of 1% CO, 2% $O_2$ 20% $H_2$, 10.0% $H_2O$, and balance $N_2$. The temperature was varied from 60 to 200 °C, with a 5-min isotherm every 20 °C.

### 2.4. Procedure for WGS and RWGS reactions

For WGS and RWGS the feeding gases mixtures were: 1% CO, 3% $H_2O$, $N_2$ to balance and 1% $CO_2$, 17% $H_2$, $N_2$ to balance, respectively, with a total flow rate of 21.0 mL/min and a GSV of 18 $L\,h^{-1}\,g_{cat}^{-1}$.

## 3. Results

### 3.1. CO oxidation in the absence of hydrogen

Under hydrogen-free CO oxidation conditions ($CO:O_2:N_2 = 1:2:97$), 4 of the 12 doped catalysts, containing the dopants Pb, V, W, and Mo, reached 100% CO conversion already at 160 °C, while the reference catalyst Pt/Ce was found less active (Fig. 1). By comparing the dopant-free 2 and 4.75 wt% Pt/Ce systems, a large positive effect of Pt loading was observed, since the highly loaded system was far the most active among the whole series.

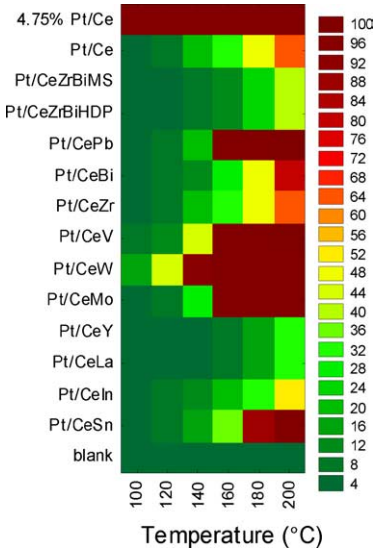


Fig. 1. CO oxidation in the absence of hydrogen: CO conversion (%) as a function of temperature (°C).

### 3.2. Selective CO oxidation in the presence of hydrogen (SelOx)

When the same catalysts were tested in the presence of hydrogen ($CO:O_2:H_2:N_2 = 1:2:20:77$), a different picture emerged (Fig. 2A). Apart from a V-containing system, which was active either in the presence or in the absence of hydrogen, other samples (with Y, In, and Zr dopants), that were inactive in the absence of hydrogen, now gave full CO conversion at temperatures < 100 °C. However, as the temperature was increased from 100 to 200 °C the CO conversion tended to decrease. With less active samples (Bi and ZrBi dopants), CO conversion begun only at 120 °C, increasing to a maximum value (not necessarily 100%) and then decreasing at higher temperatures. Unlike the hydrogen-free screening, the most active doped catalysts were found more active than the reference Pt/Ce sample, and even slightly more active than the highly loaded 4.75 wt% Pt/Ce sample. The selectivity toward $CO_2$, i.e., the percentage of oxygen consumed for oxidizing CO to $CO_2$ divided by the total amount of consumed oxygen, also depended on the ceria doping (Fig. 2B). Less active samples presented the highest selectivity toward $CO_2$, with less oxidation of hydrogen into water (note that full oxygen consumption was observed in all cases). Another trend was that the higher the temperature, the lower the selectivity toward $CO_2$.

### 3.3. Selective CO oxidation in the presence of hydrogen and water

Under industrial or pilot plant feed conditions (i.e., using a feed from the outlet of the upstream WGS reactors) the partial pressure of water is generally between 10 and 40%. We studied therefore the influence of water for all catalysts, adding 10% of water to the SelO*x* feed. Fig. 3 shows the changes in CO conversion as a function of temperature for the most active catalysts, i.e., in a domain where the conver-

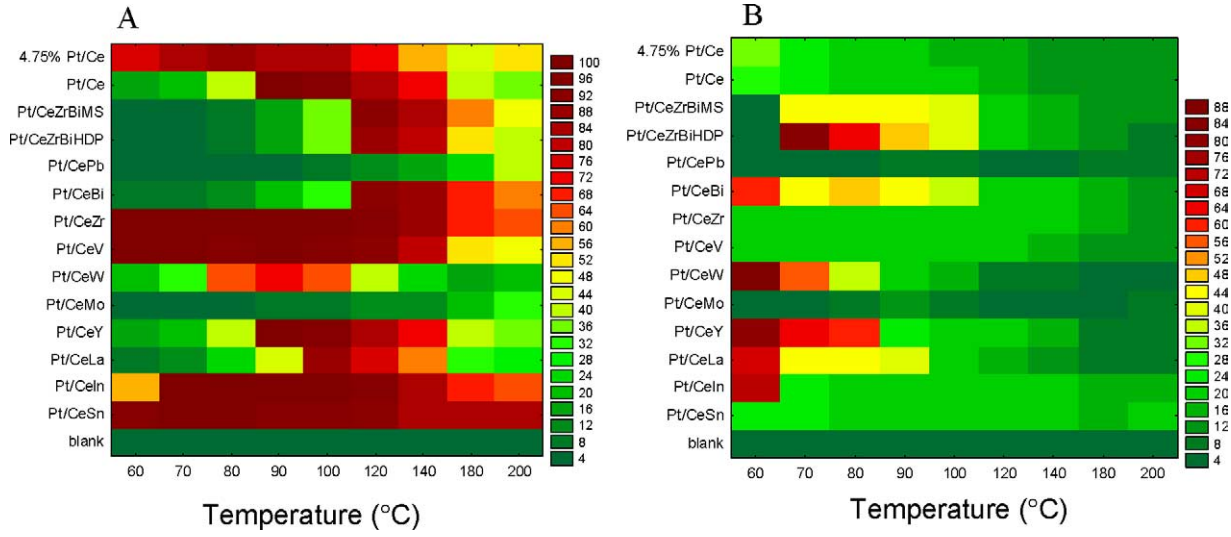


Fig. 2. CO conversion (A) and selectivity toward $CO_2$ (B) in the presence of hydrogen as a function of temperature (°C).

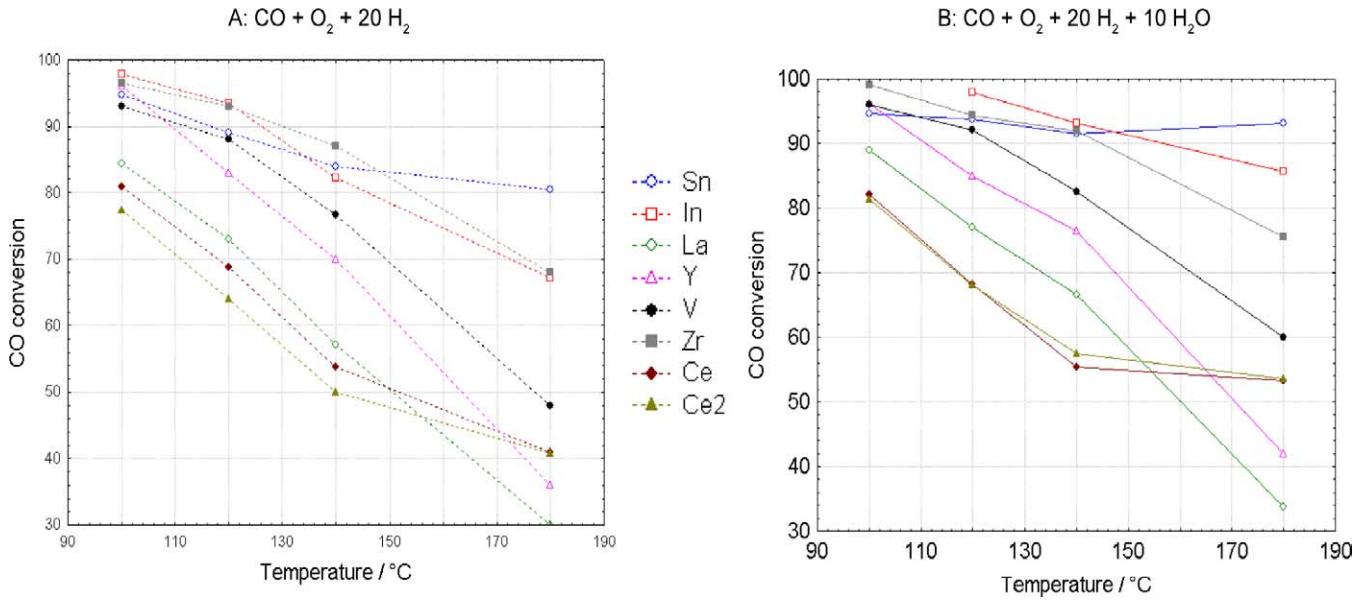


Fig. 3. Comparison of SelO$x$ performances as a function of temperature (°C) without (A) and with (B) water addition.

sion decreases with temperature, both without (Fig. 3A) and with (Fig. 3B) water addition. Adding water left the selectivity basically unchanged, but increased the CO conversion by 5–15%.

### 3.4. Water–gas shift and reverse water–gas shift reactions

During the above experiments, the catalysts were contacted with mixtures of $H_2O$, CO, $CO_2$, and $H_2$. Therefore, the gas composition may tend to equilibrate according to WGS/RWGS thermodynamics as these catalysts are also known to be active in reaching these equilibria. In the absence of added water in the feed, i.e., under "dry CO oxidation" in the presence of $H_2$ (conditions prevailing in Figs. 2 and 3A), the gas outlet concentration can be simulated by assuming that (a) a complete CO oxidation proceeds at full $O_2$ conversion within the very first part of the catalyst bed, and (b) the WGS/RWGS equilibrium is established in the remaining part of the catalyst bed (see Scheme 1). As such, if the catalyst bed is fed with a ratio of 1:2:20:77 $CO:O_2:H_2:N_2$, after full $O_2$ conversion, the remaining part of the catalyst would be contacted with a ratio of 1:3:17:77 $CO_2:H_2O:H_2:N_2$. Assuming such a mixture is totally equilibrated according to WGS thermodynamics, the backformation of CO via RWGS was calculated at the reactor exit[1] and

| Oxidation zone : | Reverse water gas shift zone : |
|---|---|
| $CO + H_2 + O_2 \rightarrow CO_2 + H_2O$ | $CO_2 + H_2 \Leftrightarrow CO + H_2O$ |

flow →

Scheme 1. Selox reactor axial mechanistic sequence.

[1] Thermodynamic calculations were performed using the Gibbs energy minimization function of the HCS Chemistry software, available from http://www.outokumpu.com/hsc.

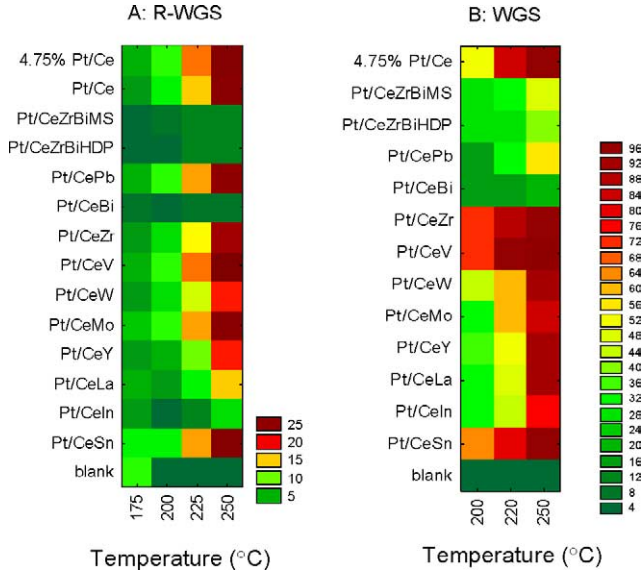


Fig. 4. Comparison of RWGS ($CO_2$ conversion, A) and WGS (CO conversion, B) performances as a function of temperature (°C).

found to be ca. 200 and 3000 ppm at 200 and 400 °C, respectively (Table 1).

To validate this simulation, we tested the activity of all the catalysts in reaching the WGS/RWGS equilibria. In a first set of experiments, the feed composition corresponding to RWGS was $CO_2:H_2:N_2 = 1:17:82$ and the reaction was performed at temperatures ranging from 100 to 250 °C. As can be seen in Fig. 4A, most catalysts gave ca. 10% $CO_2$ conversion into CO at 200 °C, with some reaching 26% conversion at 250 °C (which correspond to outlet CO concentrations of 1000 and 2500 ppm, respectively), while the calculated equilibrated values were 24% at 200 °C and 35% at 250 °C. This indicates that most of the catalysts indeed equi-

Table 1
Simulation of the SelO$x$ and RWGS processes[a]

| Reaction | Inlet composition (mol%) | | | | | | Composition after reaction/equilibrium (mol%) | | | | | | |
|---|---|---|---|---|---|---|---|---|---|---|---|---|---|
| | CO | $CO_2$ | $O_2$ | $H_2$ | $H_2O$ | $N_2$ | CO | $CO_2$ | $O_2$ | $H_2$ | $H_2O$ | $N_2$ | |
| CO and $H_2$ oxidation<br>$CO + 1/2O_2 \rightarrow CO_2$<br>$H_2 + 1/2O_2 \rightarrow H_2O$ | 1 | 0 | 2 | 20 | 0 | 77 | 0 | 1 | 0 | 17 | 3 | 79 | |
| RWGS equilibrium<br>$CO_2 + H_2 \leftrightarrow CO + H_2O$ | 0 | 1 | 0 | 17 | 3 | 79 | 0.02<br>0.30 | 0.97<br>0.69 | 0<br>0 | 16.8<br>16.7 | 3.2<br>3.3 | 79<br>79 | 200 °C<br>400 °C |

[a] On the first line (corresponding to CO and $H_2$ oxidation) the complete $O_2$ consumption is assumed, enabling CO to be completely oxidized into $CO_2$, the remaining part of oxygen being converted into $H_2O$. On the second line (corresponding to the WGS/RWGS equilibrium), the thermodynamics equilibria are calculated at 200 and 400 °C on the basis of the inlet composition, given in the left part of line 2, similar to the right part of line 1.

librate the reacting mixtures according to the WGS/RWGS thermodynamics under these conditions. In the presence of water (i.e., under more realistic SelO$x$ conditions), much less $CO_2$ to CO conversion was observed, as expected from the WGS/RWGS equilibria (0.3 and 0.6% $CO_2$ conversion at 200 and 250 °C, respectively, corresponding to outlet CO concentrations of 300 and 600 ppm, respectively).

To further examine this trend in WGS/RWGS equilibration, the catalysts were also tested for WGS activity using a feed ratio of 1:3:96 $CO:H_2O:N_2$. CO conversion was found to increase with temperature, as shown in Fig. 4B. Most catalysts gave full CO conversion, i.e., reached the WGS/RWGS equilibrium (CO conversion of 99.8 and 99.5% at 200 and 250 °C, respectively). This demonstrates the ability of ceria-based materials to equilibrate $CO/CO_2/H_2O/H_2$ mixtures, independent of the initial feed composition. Moreover, the three most active dopants for CO oxidation under hydrogen-rich conditions (Sn, V, Zr, see Fig. 4B) also gave the highest CO conversion for WGS at low temperatures.

### 3.5. Effect of contact time

If indeed RWGS takes place under SelO$x$ conditions, it must occur preferentially downstream in the reactor, i.e., after the total CO oxidation inlet zone, where the concentration of $CO_2$ is sufficient. To check this, the effect of contact time was investigated. Fig. 5 compares the changes in CO conversion with temperature as a function of contact time which was varied by using either 20 or 70 mg of 4.75% Pt/Ce, which corresponded to a bed length of 1 or 3 mm, and contact time of 48 or 170 ms, respectively (assuming a mean bed density of 0.96 g/mL). Fig. 5 also shows the thermodynamic equilibrium corresponding to the real SelO$x$ input concentration (curve Th1, which includes the values given for 200 °C in Table 1, second line, right side). In order to account for a possible adsorption of water by ceria (at least under initial testing conditions when the full adsorption capacity is not reached yet), the equilibrium was also calculated by assuming that the water formed during the initial total oxidation step (producing $CO_2$ and $H_2O$) is trapped by the ceria support (curve Th2, which corresponds to the inlet composition given in Table 1, second line, left side, but without water, i.e., $CO:O_2:CO_2:H_2O:H_2:N_2 = 0:0:1:0:17:82$ vol%).

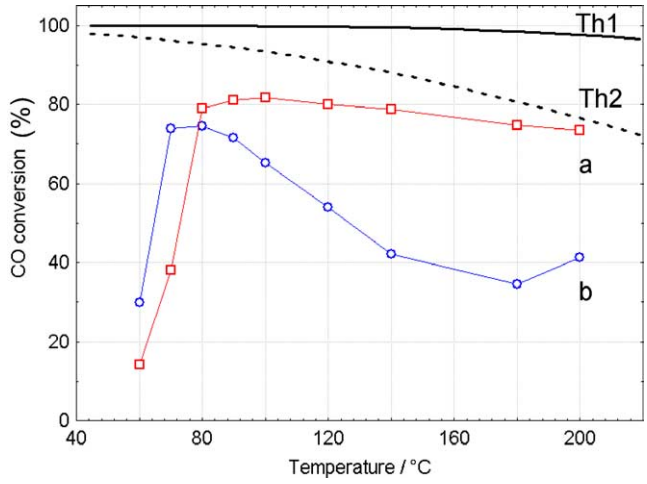


Fig. 5. Changes in CO conversion under SelO$x$ conditions as a function of temperature (°C) for two contact times (a, 170 ms; b, 48 ms). Th1, thermodynamic equilibrium for SelO$x$ inlet composition ($CO:O_2:H_2:N_2$ = 1:2:20:77 vol%); Th2, thermodynamic equilibrium for similar SelO$x$ inlet composition but assuming that the water formed by $CO/H_2$ oxidation is trapped by ceria.

Two effects are observed: (a) the light-off temperature is ca. 10 °C higher for the shorter catalyst bed, and (b) the shorter the contact time, the closer is the CO conversion to equilibrium after light-off (see Section 4).

Fig. 6 reports the changes in CO conversion keeping $W/F$ ratio (contact time) constant but varying $W$ and $F$ values. At low flow rate (curve a) the CO conversion is high at low temperature and decreases with gas inlet temperature while at higher flow rate (curve b) the CO conversion is low at low temperatures and increases as $T$ increases up to about 200 °C. In Fig. 6, the temperature measured in the middle of the catalyst bed remains always higher than the one measured at the bed inlet (from about 40 °C at low temperatures to about 20 °C at high temperatures).

### 3.6. Oxygen-storage capacity

To study further the effects of hydrogen on CO oxidation, the catalysts oxygen-storage capacity was evaluated by first oxidizing the catalyst and subsequently flowing hydrogen over it, measuring only the available surface and/or bulk

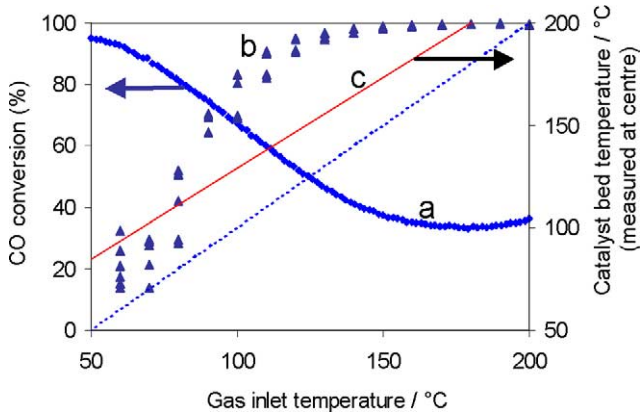


Fig. 6. Changes in CO conversion under SelO$x$ conditions over 4.75% Pt/Ce as a function of gas inlet temperature (°C) at similar contact time = 170 ms ($W/F = 2.7$) but for different $W$ and $F$ values, with curve a, $W = 70$ mg and $F = 26$ mL/min; and b, $W = 100$ mg and $F = 36$ mL/min. Inlet composition: $CO:O_2:H_2:N_2 = 1:2:20:77$ vol%. Curve c reports the temperature measured in the middle of the catalyst bed.

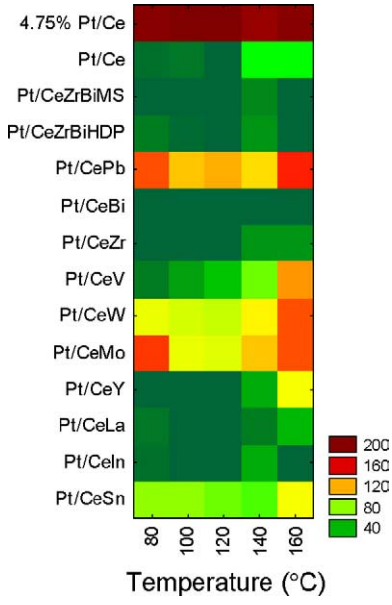


Fig. 7. Oxygen-storage capacity (μmol of hydrogen oxidized per gram catalyst) after reoxidation and flushing with Ar, as a function of temperature (°C).

oxygen [17,18]. The OSC was measured as a function of temperature for each catalyst (Fig. 7). Over the whole series, the OSC ranking was found to strictly parallel the CO oxidation ranking carried out in the absence of $H_2$ (cf. Figs. 1 and 7), the most active CO oxidation catalysts exhibiting the highest OSC, and vice versa. Moreover, the OSC values were generally independent of the temperature at this range. Above 200 °C, $H_2$ consumption increased strongly for all catalysts (in the case of La, Sn, In, and Zr dopants there was an order of magnitude difference between 200 and 160 °C).

OSC measurements carried out by using CO oxidation instead of $H_2$ did not reveal any relationship either with the CO oxidation ranking or with the SelO$x$ one (results not reported here).

## 4. Discussion

### 4.1. Effects of hydrogen on CO oxidation

The accepted mechanism for platinum-catalyzed CO oxidation assumes that both CO and $O_2$ are activated on the metal particle surface as $CO_{ads}$ and $O_{ads}$ followed by a Langmuir–Hinshelwood surface reaction between the two adsorbed species and release of $CO_2$ [19],

$$CO + * \rightarrow CO*, \quad (1)$$

$$O_2 + 2* \rightarrow 2O*, \quad (2)$$

$$CO* + O* \rightarrow CO_2 + 2*, \quad (3)$$

where $*$ is a platinum active site.

In the case of ceria-based catalysts, the support plays a key role, as the reducible ceria may also provide adsorbed oxygen species that can spill over from the support to the metal particles, the reduced $Ce^{3+}$ centerers being subsequently reoxidized by gaseous oxygen:

$$2Ce^{4+} + O^{2-} + * \rightarrow 2Ce^{3+} + O*, \quad (4)$$

$$2Ce^{3+} + 1/2O_2 \rightarrow 2Ce^{4+} + O^{2-}. \quad (5)$$

In the presence of hydrogen, competition between $H_2$ oxidation and CO oxidation is likely to influence the equilibria at the surface. One option is for hydrogen to adsorb on the Pt sites, competing with CO activation:

$$H_2 + 2* \rightarrow 2H*, \quad (6)$$

$$O_2 + 2* \rightarrow 2O*, \quad (7)$$

$$2H* + O* \rightarrow H_2O + 2*. \quad (8)$$

Hydrogen may also react directly with ceria lattice oxygen (Eq. (9)), creating an anionic vacancy and increasing the mobility of the remaining lattice oxygen atoms. The resulting hydroxyl anions can combine to give water and $O^{2-}$ (Eq. (10)) with the $Ce^{3+}$ cations reoxidized by molecular oxygen to $Ce^{4+}$ as above:

$$2Ce^{4+} + 2O^{2-} + H_2 \rightarrow 2Ce^{3+} + 2OH^-, \quad (9)$$

$$2OH^- \rightarrow H_2O + O^{2-}. \quad (10)$$

Doping the fluorite structure with different cations may induce various structural effects, such as promoting the creation and/or *stabilization* of oxygen vacancies [13] and modifying surface acidity and basicity, these effects being likely to interact on the oxygen diffusion. The latter is usually limited to surface diffusion for undoped ceria (bulk diffusion can also be considered after Zr addition [20]). Therefore, doping can change the above elementary steps for CO oxidation which involve ionic oxygen migration and diffusion.

### 4.2. CO oxidation in the absence of hydrogen

Catalysts activity for CO oxidation in the absence of hydrogen parallels strictly their OSC. This indicates that the activated oxygen required for reacting with adsorbed carbon monoxide on Pt is provided by oxygen spillover from ceria and not from gaseous oxygen activation on Pt. Hence, the rate-determining step (RDS) for CO oxidation appears to be the surface diffusion of oxygen from ceria to platinum, which agrees with the fact that the OSCs are almost independent of the reaction temperature (Fig. 7). The large increase in OSC noted for all systems at 200 °C and above may reflect the direct reduction of ceria by hydrogen at these temperatures.

The most performing systems both for CO oxidation in the absence of hydrogen and for OSC (measured by hydrogen oxidation) were found to contain Pb, V, W, and Mo ceria doping cations. A common feature for these cations is that the most stable forms of the corresponding oxides are essentially amphoteric or acid except V, which can be either acid or basic. By maintaining an optimized level of surface acidity, these dopants would somehow neutralize ceria basicity (hydroxyl groups) and therefore inhibit formation of stable adspecies such as formates and carbonates which would, in turn, inhibit oxygen mobility and spillover toward activated CO on platinum particles (Eq. (4)) [20].

Another effect was clearly related to the content of Pt, high loading favoring CO oxidation and OSC. This may suggest that within the RDS of surface diffusion of oxygen from ceria to platinum, the number of interfacial metal atoms (linked to the concentration of particles and their mean size) plays also a major role in the overall rate of reaction.

Finally, the absence of any clear relationship between CO oxidation and OSC measured by CO oxidation would indicate that in the absence of a continuous source of oxygen, CO activated on Pt particles may also migrate toward the ceria surface to react with OH groups for forming formate species, as clearly revealed by in situ DRIFT studies carried out on similar systems [21,22]. Thus more complex processes involved in OSC-CO measurements rule out any simple relationship with CO oxidation.

### 4.3. CO oxidation in the presence of hydrogen (SelOx)

The change in the catalysts CO oxidation ranking in the presence of hydrogen (SelO$x$ conditions) indicates that the RDS of oxygen surface diffusion is affected. Contrary to the previous analysis for CO oxidation in the absence of hydrogen or OSC, it appears that most of the best ceria dopants for SelO$x$—V, In, Sn, Zr, and Y—are essentially basic oxides in their stable form, except again V, which can be both acidic or basic, depending on its state of valence. By generating or stabilizing basic OH groups on ceria surfaces in place of oxygen vacancies, these cations would therefore limit oxygen mobility and spillover, which, in turn, could tune the competition between CO and $H_2$ for being oxidized at interfacial sites. The effect of these dopants could also be analyzed as preventing efficiently ceria surface from being reduced by hydrogen (Eq. (9)), possibly by providing extra sources of ionic oxygen, either from the bulk (for Ce/Zr systems) or via heterovalent substitution. Very little change in the selectivity was observed after adding water to the SelO$x$ system, which may be explained by the fact that OH groups are already present on ceria surface under "dry" SelO$x$ conditions (water formed only from hydrogen oxidation).

### 4.4. WGS/RWGS equilibria

Except for Eq. (2), we can consider the elementary reactions shown above to be partially reversible. A summation of these steps corresponds essentially to the WGS equilibrium. This explains why the most efficient SelO$x$ catalysts also perform well in equilibrating WGS mixtures. A direct consequence is that under a hydrogen-rich SelO$x$ atmosphere, after CO has been oxidized to $CO_2$, it can reform by RWGS. This is clearly demonstrated in the simulations and in the contact time experiments shown in Fig. 5. However, for the latter (carried out in the absence of added water), the outlet CO concentration was much higher than expected from the RWGS thermodynamics, especially for longer contact times (longer bed lengths). This effect can most probably be assigned to a temperature rise within the reactor due to the exothermic initial CO and $H_2$ oxidation. As a matter of fact, this effect is clearly revealed in Fig. 6 where the temperature within the bed is found to be about 40 °C higher than the inlet temperature for a low gas flow rate, which corresponded to a high initial conversion of CO and then decreasing at higher temperatures (curve a). For a higher flow rate (curve b), the conversion profile was now increasing with temperature as expected for an activated oxidation process. This latter profile may be assigned to a better heat transfer from the bed to the outlet effluents. Thus, at high contact time (Fig. 5, curve a) or low overall flow rate (Fig. 6, curve a), the temperature rise due to CO oxidation would expand to the WGS/RWGS downstream zone and favor the RWGS equilibrium (Scheme 1) and explain a higher outlet CO concentration. In addition, higher temperature in the oxidation zone might also favor the oxidation of $H_2$ at the expense of CO oxidation due to CO desorption, which would also contribute to higher outlet CO concentration by decreasing CO vs $H_2$ oxidation selectivity.

In addition to the above temperature effects, a transient trapping effect of water by ceria (occurring under the fast parallel testing conditions before steady state is achieved) could reinforce RWGS equilibrium displacement toward CO formation. If we assume that the water produced by the $CO/H_2$ initial oxidation is even partly trapped by ceria, then the experimental CO conversion becomes much closer to the thermodynamic equilibrium for the case of short contact times (cf. curves a and Th2 in Fig. 5). For longer contact times (Fig. 5, curve b), the water formed by the RWGS reaction could also be trapped, which would further increase

the $CO_2$ to CO conversion, as observed experimentally. Indeed for catalytic measurements carried out after adsorption steady state has been achieved, this effect could not be considered anymore. Further experiments are in progress to unravel the various effects above described for a better process control.

### 4.5. *High-throughput catalyst discovery—Pros and cons*

Finally, it is worthwhile to consider the investigation method employed here, namely, the use of high-throughput equipment for the extraction of mechanistic information. In this study, more than 600 experiments were performed in 3 weeks. In contrast to the usual two-stage "discovery" and "optimization" approach, we used the high-throughput system in a manner similar to conventional catalysis investigations [23]. This means that only the first set of experiments was designed a priori, whereas the following sets were each designed in light of the previous results. It should be pointed out that data processing was a rate-limiting step even though specialized VisualBasic routines were used.

This modus operandi is not merely about saving time. In the traditional combinatorial approach [24–26] it is generally considered that selection of performing elemental combinations can be performed in the so-called primary screening (discovery stage) where testing conditions are often simplified to speed up the screening process. Then, in the second stage (lead optimization), hits from the first screening are tested under more realistic conditions. This, however, can lead to major errors: if, to accelerate the initial screening, the discovery of new SelO$x$ catalysts had been carried out in the absence of hydrogen (or just by performing the even faster OSC measurements), the ranking information obtained would have been totally misleading!

Another point relates to data quality and meaning for complex and intricate reactions like the ones studied here: from the contact time experiments we can see that the risks for data misinterpretation when high-throughput experiments are carried out without satisfactory control of temperature and pressure conditions are high (including possibly transient adsorption effects).

The choice of the discovery test reactions is therefore crucial. One option, as shown here, is to try and test sets of diverse catalyst formulations combined with real-time performance analysis, including transient experiments (like for OSC measurements). Robots are available for doing the experiments, but the bottleneck lies now with the data analysis and processing. Optimizing the methods for high-throughput data management including kinetic data obtained under non-stationary conditions [27] is now the primary objective if we use high-throughput technologies to discover new catalysts.

## 5. Conclusions

Ceria-based supports doped with small amounts of heteroatom cations show, despite their almost identical crystal X-ray structures and compositions, diverse redox properties and catalytic activity in CO oxidation, with and without hydrogen, and under water–gas shift conditions. The nature of the dopant was found to strongly influence the performance of Pt/ceria catalysts, both for CO oxidation in the presence or absence of hydrogen and OSC, measured by hydrogen oxidation. Common features like basicity or acidity of the most stable oxide forms of the doping cations seem to play a major role in systems performances, most likely by modifying surface oxygen migration: acidic/amphoteric cations tend to favor both CO oxidation in the absence of hydrogen and OSC, while basic cations tend to favor SelO$x$ reaction. However, a cation like vanadium, able to accommodate both acidic or basic state, is beneficial in all cases. This statement points out the limits of oversimplified relationships between dopant nature and catalytic performances.

WGS/RWGS equilibria must be considered in addition to the oxidation processes. This was affirmed by both experiments and simulations. Therefore, because they are also active in the WGS/RWGS equilibration, the most active ceria-supported Pt catalysts must be used as SelO$x$ catalysts at low temperatures and short contact times. Further research to optimize the CO oxidation performance in the presence of hydrogen by combining diverse supports with various noble and transition metals is under progress in our laboratories.

## Acknowledgments

Part of this work was supported by the EC program COMBICAT (GRRD-CT 1999-00022) and D.T. fully acknowledges the EC program Marie Curie Host Fellowships (HPMT-CT-2000-00160) for granting his stay at IRC. AMTEC GmbH is fully acknowledged for having supported part of the parallel reactor development, now commercialized as SWITCH 16 reactor (http://www.amtec-chemnitz.de).

## References

[1] L. Carrette, K.A. Friedric, U. Stimming, Chem. Phys. Chem. 1 (2000) 162–193.
[2] R.M. Ormerod, Chem. Soc. Rev. 32 (2003) 17–28.
[3] L.P.L. Carrette, K.A. Friedrich, M. Huber, U. Stimming, Phys. Chem. Chem. Phys. 3 (2001) 320–324.
[4] J.J. Baschuk, X. Li, Int. J. Energy Res. 25 (2001) 695–713.
[5] T.V. Choudhary, D.W. Goodman, Top. Catal. 21 (2002) 25–34.
[6] H. Häkinnen, S. Abbet, A. Sanchez, U. Heiz, U. Landman, Angew. Chem., Int. Ed. 42 (2003) 1297–1300.
[7] A.K. Santra, D.W. Goodman, Electrochim. Acta 47 (2002) 3595–3609.
[8] I. Langmuir, Trans. Faraday Soc. 17 (1922) 672–675.
[9] J.K. Nørskov, Nature 414 (2001) 405–406.
[10] Y. Zhang-Steenwinkel, J. Beckers, A. Bliek, Appl. Catal. A 235 (2002) 79–92.
[11] S.D. Park, J.M. Vohs, R.J. Gorte, Nature 404 (2000) 265–267.
[12] A.E.C. Palmqvist, M. Wirde, U. Gelius, M. Muhammed, Nanostruct. Mater. 11 (1999) 995–1007.
[13] G. Rothenberg, E.A. de Graaf, A. Bliek, Angew. Chem., Int. Ed. 42 (2003) 3066–3068.

[14] M. Mogensen, N.M. Sammes, G.A. Tompsett, Solid State Ionics 129 (2000) 63–94.
[15] G.S. Li, R.L. Smith, H. Inomata, J. Am. Chem. Soc. 123 (2001) 11,091–11,092.
[16] C. Mirodatos, Y. Schuurman, C. Hayaud, A. Holzwarth, D. Farrusseng, T. Richter, EP 1 293 772 A2, 2003, to CNRS-AMTEC GmbH.
[17] R.K. Grasselli, D.L. Stern, J.G. Tsikoyiannis, Appl. Catal. A 189 (1999) 1–8.
[18] R.K. Grasselli, D.L. Stern, J.G. Tsikoyiannis, Appl. Catal. A 189 (1999) 9–14.
[19] M. Boudart, in: H. Knözinger, J. Weitkamps (Eds.), Handbook of Heterogeneous Catalysis, vol. 3, Wiley–VCH, Weinheim, 1997, p. 958.
[20] C. Descorme, Y. Madier, D. Duprez, J. Catal. 196 (2000) 167.
[21] E. Odier, C. Marquez-Alvarez, L. Pinaeva, Y. Schuurman, C. Millet, C. Mirodatos, Stud. Surf. Sci. Catal. 136 (2001) 483–488.
[22] E. Odier, Y. Schuurman, H. Zanthoff, C. Millet, C. Mirodatos, Stud. Surf. Sci. Catal. 133 (2001) 327–332.
[23] G. Rothenberg, H.F.M. Boelens, D. Iron, J.A. Westerhuis, Chim. Oggi 21 (2003) 80–83.
[24] D. Farrusseng, L. Baumes, C. Hayaud, I. Vauthey, P. Denton, C. Mirodatos, in: E.G. Derouane, E.G. Derouanes (Eds.), NATO Science Series II: Mathematics, Physics and Chemistry, vol. 69, Kluwer Academic, Dordrecht, 2001, pp. 101–124.
[25] D. Farrusseng, L. Baumes, C. Mirodatos, in: R.A. Potyrailo, E.J. Amiss (Eds.), High-Throughput Analysis: A Tool for Combinatorial Materials Science, Kluwer Academic, Dordrecht, 2003, pp. 551–579.
[26] G. Rothenberg, H.F.M. Boelens, D. Iron, J.A. Westerhuis, Chem. Eur. J. 9 (2003) 3876–3881.
[27] A.C. van Veen, D. Farrusseng, M. Rebeilleau, T. Decamp, A. Holzwarth, Y. Schuurman, C. Mirodatos, J. Catal. 216 (2003) 135–143.